



Cite this: *Nanoscale Adv.*, 2023, 5, 5295

A nanoscale study of the structure and electrical response of *Sepia eumelanin*[†]

Dieudonné Niyonkuru,[‡][†]^a Anthony Camus,[‡][†]^a Manuel Reali,^a Zhaojing Gao,^a Daniel M. Shadrack,[‡]^b Oleg Butyaev,^c Marko Surtchev,[‡]^c and Clara Santato [‡]^a^{*}

Eumelanin, the brown-black member of the melanin biopigment family, is a prototype material for sustainable (green) organic electronics. *Sepia eumelanin* (*Sepia*) is a type of biosourced eumelanin extracted from the ink sac of cuttlefish. Electron microscopy and scanning probe microscopy images of *Sepia* show distinguishable near spherical granules with diameters of about 150–200 nm. We have recently reported on predominant electronic transport in printed films of *Sepia* formulated inks including the (insulating) binder Polyvinyl-butylal (PVB). In that work, we proposed that inter-granular percolative transport, observed for micrometric interelectrode distances, is promoted by the confining action of the PVB binder on the *Sepia* granules. Considering that inter-granular transport implies intra-granular transport, in this work we proceeded to a nanoscale study of *Sepia* granules by High Resolution Atomic Force Microscopy (HR-AFM) and Conductive-AFM (c-AFM). We have observed protrusions on the surface of the *Sepia* granules, suggesting sub-granular structures compatible with the hierarchical development of *Sepia*, as proposed elsewhere. For films of *Sepia* formulated inks deposited on gold-coated substrates, c-AFM revealed, for the very first time, a nanoscale electrical response. Nanoscale studies provide the key to structure–property relationships in biosourced materials strategic for sustainable organic electronics.

Received 24th May 2023
Accepted 22nd August 2023

DOI: 10.1039/d3na00355h
rsc.li/nanoscale-advances

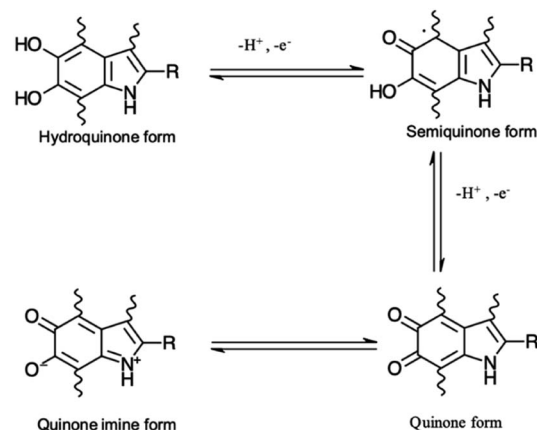
Introduction

Melanins are a family of biopigments which exhibit potentially useful functional properties, including UV photoprotection, metal ion-binding affinity, free radical quenching, redox activity, hydration-dependent electrical response.^{1–5} Among melanins, eumelanin is a brown-black type found in invertebrates, such as cephalopods and insects, and vertebrates, including humans. *Sepia eumelanin* (indicated as *Sepia* in what follows) is extracted from the ink sac of cuttlefish.¹

Eumelanin is an environmentally benign material for sustainable (green) organic electronics, a promising route to improve the environmental footprint of the electronics sector. Sustainable organic electronics is based on the use of abundant electro- and photo-active materials readily available from biomass feedstock, or novel production schemes involving non-toxic materials (through green chemistry processes), and eco-

design of devices that includes environmentally acceptable end-of-life scenarios, such as composting.^{6–8}

Eumelanin may be synthesized by the oxidative polymerization of the monomers 5,6-dihydroxy indole (DHI) and 5,6-dihydroxy indole-2-carboxylic acid (DHICA). Different redox forms (hydroquinone (reduced redox form), semiquinone (intermediate form) and quinone (oxidized form)) are possible in the macromolecule (Fig. 1).



^aDepartment of Engineering Physics, Polytechnique Montréal, C.P. 6079, Succ. Centre-Ville, Montréal, QC H3C3A7, Canada. E-mail: clara.santato@polymtl.ca

^bDepartment of Chemistry, St. John's University of Tanzania, P.O. Box 47 Dodoma, Tanzania

^cNT-MTD Spectrum Instruments, 5861 S Kyrene Rd#19, Tempe, AZ 85283, USA

† Electronic supplementary information (ESI) available. See DOI: <https://doi.org/10.1039/d3na00355h>

‡ Authors that equally contributed to this work.



These monomers have several polymerization sites, so that eumelanin is a chemically disordered (heterogeneous) macromolecule. This leads to polymorphic π – π stacked regions in the supramolecular structure, such that eumelanin exhibits structural (and consequently energetic) disorder.

Eumelanin exhibits a hierarchical structure.⁹ Ensembles of oligomers of DHI and DHICA building blocks (protomolecules) build up *via* π – π stacking of about 4–5 planes, with an inter-plane distance of about 3.4 Å and lateral extension of about 20 Å.^{10–12} Physical interactions among such protomolecules generate 10–15 nm-sized structures, observed by Scanning Electron Microscopy (SEM) and Atomic Force Microscopy (AFM).^{13–16} Large particles, of 100–200 nm, form from further aggregation, through π – π stacking and edge-to-edge H-bonding interactions. Such large particles can be associated with granules observed by Transmission Electron Microscopy (TEM), SEM or AFM images obtained from Sepia.^{13–18} Sepia is the type of eumelanin that can be isolated from the ink sac of cuttlefish using protocols that differently affect its chemical and structural properties.^{1,17,19}

We have recently observed electronic transport in films flexographically printed from formulations including Sepia and the (insulating) organic binder PVB,²⁰ and the measured conductivity is as high as 10^{-3} S cm⁻¹. Such values are typical for synthetic high-performance organic electronic polymers but quite uncommon for biosourced materials.^{21–23} We proposed that inter-granular percolative transport in Sepia is enhanced due to the confining action of the PVB binder on the Sepia granules, whose proximity would induce the formation of conductive paths. We also discussed the hypothesis that inter-granular transport implies intra-granular transport.

Here, we report on a study of Sepia by High-Resolution AFM (HR-AFM) and Conductive-AFM (c-AFM), to shed light on its structure and functional properties (electrical response), at the nanoscale. Studies were performed both on bare Sepia and on Sepia blended with the binder PVB. The topography of the Sepia granules includes protuberances that we tentatively attribute to sub-granular structures due to the hierarchical development of Sepia.²⁴ HR-AFM permitted the quantitative evaluation of these protuberances. Using c-AFM, we have made the first observation of nanoscale charge carrier transport in Sepia.

Experimental methods

Extraction of Sepia

Raw cuttlefish ink (Stareef Seafood Boston, product of Spain) was purchased in a Montreal fish market. Sepia powder was extracted using a previously reported extraction protocol.^{19,20} Briefly, 300 g of raw ink was suspended in 500 mL of HCl (2 M, Acros Organics). The suspension was stirred at room temperature for 24 hours, sequentially centrifuged (Allegra X-30R centrifuge, Beckman Coulter) and dispersed as follows: three times with HCl (0.5 M), once with de-ionized (DI) water, once with a buffer solution (0.02% v/v of monobasic sodium phosphate (200 mM, Sigma Aldrich), 32.49% v/v of dibasic sodium phosphate (200 mM, Sigma Aldrich) and 67.49% v/v of

DI water), once with ethanol (Sigma Aldrich), once with DI water and finally once with ethyl acetate (Sigma Aldrich), for a total of 10 steps. To remove excess ethyl acetate after centrifugation, the solid was rinsed, dispersed and centrifuged four times with DI water. Each centrifugation step was performed at 10 000 rpm at 5 °C for different duration times (15 min for HCl 2 M, HCl 0.5 M, ethanol, and ethyl acetate, 25 min for DI water and the buffer solution). Finally, the extracted powders were lyophilized for 24 hours at –80 °C to remove excess water. Fine black Sepia melanin powders were obtained and manually ground to break large agglomerates. This extraction procedure provided 30 to 35 g of fine powders from 300 g of initial raw ink.

Sepia formulated ink

The preparation of the ink formulation was inspired by the formulation reported in ref. 20, where the ink consisted of a blend of 64.8% w/w of 1-propanol (Sigma Aldrich), 19.1% w/w of Sepia powder, 11.4% w/w of Polyvinyl-butylal (PVB, B-30HH, MOWITAL®), 4.4% w/w of 1-methoxy-2-propanol (Sigma Aldrich) and 0.3% w/w of TEGO® Wet KL 245 polyether siloxane copolymer (Evonik). 1-Propanol and PVB were mechanically stirred at 600 rpm for 20 min. Afterwards, Sepia melanin was gradually added and mixed for 24 hours at 2750 rpm in an attritor consisting of a high-rotation speed disk and zirconium oxide beads with a diameter of 1 mm, in a cooled vessel. The ink (with Sepia powder to PVB mass ratio is 62/38% w/w) was obtained by adding 1-methoxy-2-propanol and TEGO® Wet KL 245. Differently from ref. 20, in this work the Sepia powder/PVB ratio was finally adjusted to 92/8% w/w by adding Sepia powders to the 62/38% w/w ink.

Preparation of substrates and samples

Two sets of samples were prepared, using Sepia powder and Sepia formulated ink (92/8% w/w, Table S1†). The powder was drop-cast from an ethanol suspension whereas the formulated ink was spin-coated (6000 rpm, 40 s) on gold-coated SiO₂ substrates (40 nm-thick Au, e-beam deposited on wet thermal oxide grown on the polished front side of a (1-0-0) Si wafer). Drop cast Sepia samples are shown in Fig. 2 and 3, respectively. Spin-coated films from Sepia formulated ink are reported in Fig. 4.

Atomic force microscopy (AFM) and conductive AFM (c-AFM)

The AFM images were acquired using the NTEGRA SPM system (NT-MDT Spectrum Instruments) in scanning by the sample configuration equipped with active anti-vibration protection. AFM (topography) images were collected in amplitude modulation (AM) mode. C-AFM images were collected in Hybrid (HD) mode by applying 2 V between the gold substrate coated with the film and the Pt-coated AFM probe (with tip radius of about 35 nm). The c-AFM technique requires mechanical stability of the material studied upon scanning of the conductive tip. We therefore used a binder to enhance the adhesion and stability of the Sepia melanin granules on the gold-coated SiO₂ substrate. Six samples of spin-coated Sepia formulated ink and one



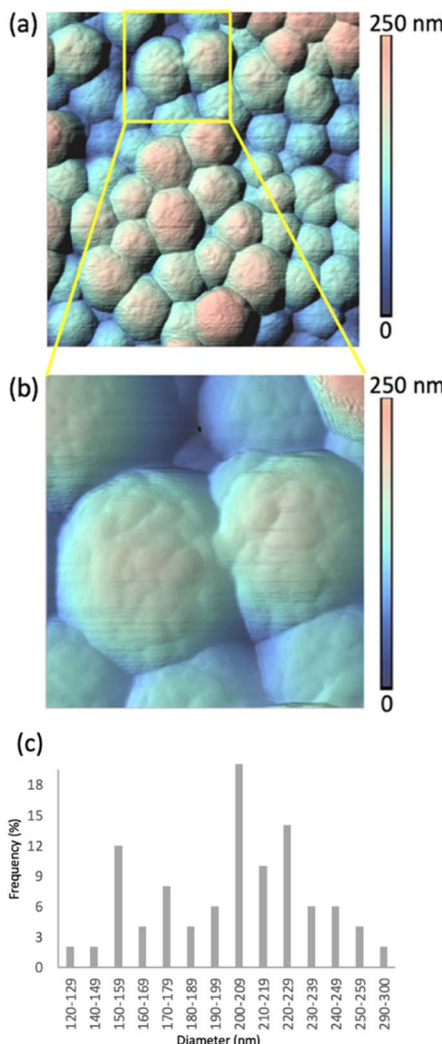


Fig. 2 AFM images of drop cast Sepia on gold-on-SiO₂: (a) 1.2 μm × 1.2 μm-sized and (b) 400 nm × 400 nm-sized (corresponding to the square in (a)). (c) Histogram showing the distribution of the diameters of the Sepia granules.

sample of drop-cast Sepia were characterized by AFM and three of these samples were characterized with c-AFM (see details in Table S1 shown in the ESI†).

Data analysis

The AFM data analysis was performed using Image Analysis software (NT-MDT Spectrum Instruments). To measure granule diameters, we analyzed 50 granules with distinguishable boundaries. For each granule, two or three measurements were taken and averaged (see Fig. S1 ESI†). Relative heights on the granule surface' profile were plotted and fitted by assuming a spherical shape for the granules, using Python software. Each line gives a profile corresponding to an arc of a circle belonging to the sphere (Fig. 3(a)). Such a circle contains the points corresponding to the minima of the protrusions (blue cross-points in Fig. 3(b)). The polynomial fitting equation is therefore given by:

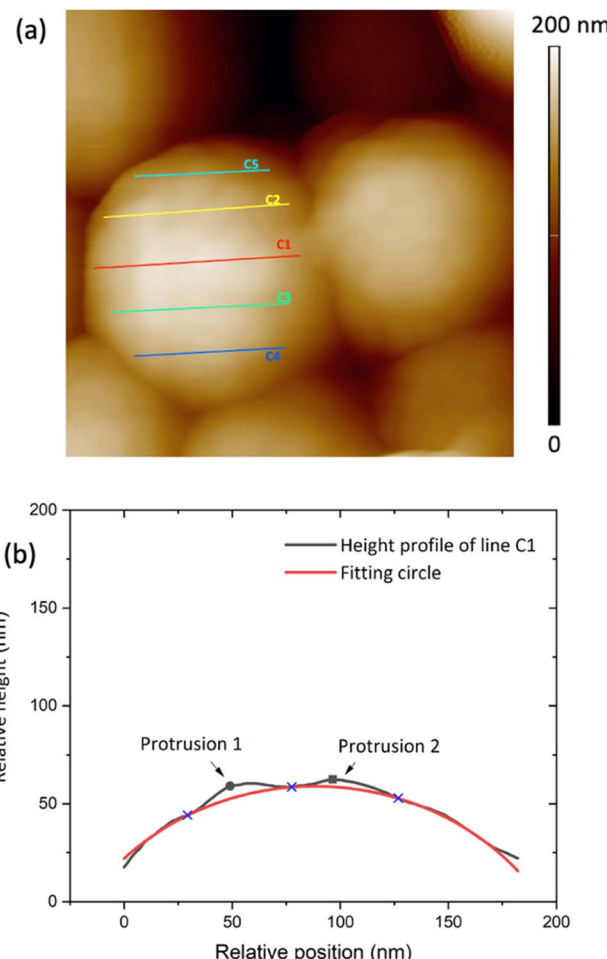


Fig. 3 (a) 400 nm × 400 nm AFM image of Sepia drop cast on Au-on-SiO₂, (b) relative height of the surface profile associated with line C1 on the granule in (a).

$$(x - x_0)^2 + (y - y_0)^2 = r^2 \quad (1.0)$$

where $x, y, (x_0, y_0)$, and r are the relative position of each point of the line, the relative height of the point on the granule surface, the coordinates associated with the center of the fitting circle, and its radius, respectively. The height of each protrusion is therefore deduced as the distance between the highest point in the protrusion and the center of the fitting circle (x_0, y_0) minus the radius r . Then, the width of the protrusion is measured at half of the height of the protrusion (*i.e.*, the Full Width at Half Maximum (FWHM)).

Results and discussion

Fig. 2 shows HR-AFM images of Sepia drop-cast on Au-on-SiO₂ substrates from ethanol solutions. The lower magnification image in Fig. 2(a) and the higher magnification in Fig. 2(b), along with the color-coded heights, indicate nearly spherical granules, with diameters in the range of 120 to 300 nm, given in the histogram in Fig. 2(c). This is in agreement with previous reports.^{13–16,18}

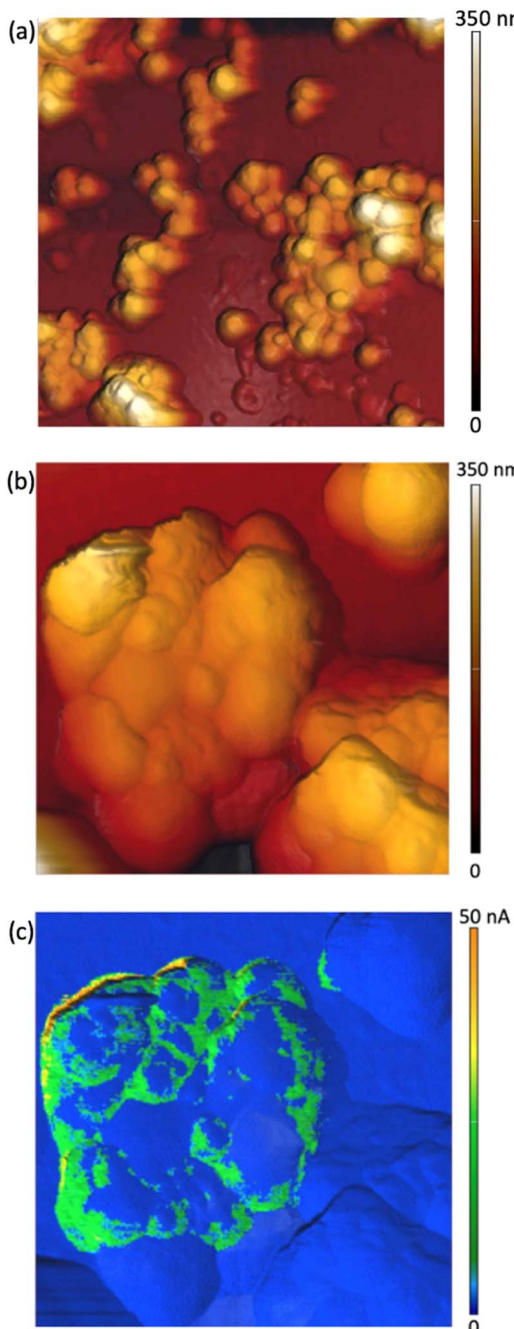


Fig. 4 AFM images of Sepia-PVB films: (a) $3\text{ }\mu\text{m} \times 3\text{ }\mu\text{m}$ -sized, (b) $1\text{ }\mu\text{m} \times 1\text{ }\mu\text{m}$ -sized and (c) current image corresponding to the AFM image in (b).

The HR-AFM images reveal the complex topography of the granules, involving the presence of surface protrusions. We proceeded to a quantitative evaluation of the width and height of such protrusions (see Experimental methods, Fig. S2, S3 and Table S2†). Our evaluation suggests that the widths of the surface protrusions are between 6.0 and 40.9 nm, with the highest frequency in the distribution (64%) for widths between 11.0 and 20.9 nm (Fig. S3a†). The heights of the protrusions are between 1.0 and 7.9 nm, with about 80% of the measured

heights being between 1.0 and 3.9 nm (Fig. S3b†). The average width and height are evaluated at 18.5 ± 6.4 nm and 3.0 ± 1.6 nm, respectively.

Considering the size of the protrusions, we hypothesize that they belong to aggregates of protomolecules.^{13–16,24} Therefore, our observations corroborate the hierarchical model describing the development of Sepia's nanostructure. The widths and heights of the protrusions relate to the quality of the molecular and supramolecular development in Sepia, as associated with planar/twisted structural segments and intermolecular interactions, such as π – π stacking, cation– π interactions and H-bonding.^{25–27}

With a long term goal of shedding light on the dependence of Sepia charge carrier transport properties on the distance range probed, we performed a c-AFM study. For this purpose, we spin-coated samples from Sepia formulated ink (see Experimental methods), to ensure their stability under mechanical contact of the c-AFM tip.

AFM images of Sepia-PVB samples confirm the presence of nearly spherical granules (Fig. 4(a) and (b)). The difference in topography between samples in Fig. 2 and 4 is attributable to the PVB insulating binder, which is part of the ink in the latter case, thus partially covering the surface of the samples.

The c-AFM images show the presence of c-AFM tip-to-Sepia-to-gold conductive paths (Fig. 4(c)). We were therefore successful in observing, for the very first time, the electrical response of Sepia, at the nanoscale. The inhomogeneity of the samples' conductivity (Fig. 4(c)) can be attributed to the presence of the binder at the interface between the AFM probe and the Sepia melanin granules.

The c-AFM images show that there are many areas on the granules which are conductive. These are preferentially located at the boundaries between Sepia granules, regions where the PVB binder is likely to be present in lower amounts than elsewhere. This hypothesis is in agreement with the recent observation of the confining action of the PVB binder; such action permits charge carrier percolation in printed films of Sepia formulated ink.²⁰

Conclusions and perspectives

In the context of our efforts to probe charge carrier transport at different length scales for natural materials exhibiting structural hierarchy, we have conducted a nanoscale scanning probe study on the biopigment Sepia eumelanin, a prototype material in sustainable organic electronics. Such studies are needed to establish sound structure–properties relationships, required to eco-design sustainable organic (opto)electronic devices. HR-AFM images of Sepia, in accordance with previously reported results, indicated nearly spherical granules with diameters in the range of 120–300 nm. The images also revealed the presence of protrusions on the surfaces of the granules, with average width and height being evaluated at 18.5 ± 6.4 nm and 3.0 ± 1.6 nm, respectively. This last observation is compatible with the hierarchical development model of Sepia, where protrusions might be portions of sub-granular structures *i.e.* sub-units of the Sepia granules.



c-AFM images of Sepia formulated ink films (where Sepia is blended with the PVB binder) exhibited conductive regions attributable to AFM tip to Sepia to gold paths, supporting the intra- and inter-granular percolation model proposed in ref. 20.

Work is in progress to deposit Sepia granules on nano-scaled pre-patterned substrates fabricated using e-beam lithography for the study of intra-granular transport at interelectrode distances of about 100–200 nm. In perspective, we plan to explore the effect of the type of biosource and extraction routes on the morphology and functional properties of Sepia.

Author contributions

This experiment was conceived by C. S. The AFM and c-AFM images were collected by M. S. and O. B. Samples were prepared by A. C. and D. N. Data analysis was performed by D. N., Z. G. M. S, M. R., A. C., and C. S. All the authors contributed to the manuscript writing.

Conflicts of interest

There are no conflicts of interest to declare.

Acknowledgements

This work was financially supported by the Natural Sciences and Engineering Research Council of Canada (NSERC, Discovery Grant C. S). We thank Prof. A. Yelon for fruitful discussions.

References

- 1 M. d'Ischia, K. Wakamatsu, A. Napolitano, S. Briganti, J. C. Garcia-Borron, D. Kovacs, *et al.*, Melanins and melanogenesis: methods, standards, protocols, *Pigm. Cell Melanoma Res.*, 2013, **26**(5), 616–633.
- 2 M. d'Ischia, A. Napolitano, A. Pezzella, P. Meredith and M. Buehler, Melanin Biopolymers: Tailoring Chemical Complexity for Materials Design, *Angew Chem. Int. Ed. Engl.*, 2020, **59**(28), 11196–11205.
- 3 E. Di Mauro, R. Xu, G. Soliveri and C. Santato, Natural melanin pigments and their interfaces with metal ions and oxides: emerging concepts and technologies, *MRS Commun.*, 2017, **7**(2), 141–151.
- 4 X. Wang, L. Kinziabulatova, M. Bortoli, A. Manickoth, M. A. Barilla, H. Huang, *et al.*, Indole-5,6-quinones display hallmark properties of eumelanin, *Nat. Chem.*, 2023, **15**, 787–793.
- 5 M. Reali, A. Gouda, J. Bellemare, D. Menard, J. M. Nunzi, F. Soavi, *et al.*, Electronic Transport in the Biopigment Sepia Melanin, *ACS Appl. Bio Mater.*, 2020, **3**(8), 5244–5252.
- 6 F. Torricelli, I. Alessandri, E. Macchia, I. Vassalini, M. Maddaloni and L. Torsi, Green Materials and Technologies for Sustainable Organic Transistors, *Adv. Mater. Technol.*, 2021, **7**(2), 2100445.
- 7 M. Baumgartner, M. E. Coppola, N. S. Sariciftci, E. D. Glowacki, S. Bauer and M. Irimia-Vladu, Emerging "Green" Materials and Technologies for Electronics, *Green Mater.*, 2018, **101**, 1–5.
- 8 E. Di Mauro, D. Rho and C. Santato, Biodegradation of bio-sourced and synthetic organic electronic materials towards green organic electronics, *Nat. Commun.*, 2021, **12**(1), 3167.
- 9 M. d'Ischia, A. Napolitano, A. Pezzella, P. Meredith and T. Sarna, Chemical and structural diversity in eumelanins: unexplored bio-optoelectronic materials, *Angew Chem. Int. Ed. Engl.*, 2009, **48**(22), 3914–3921.
- 10 G. W. Zajac, J. M. Gallas, J. Cheng, M. Eisner, S. C. Moss and A. E. Alvarado-Swaisgood, The fundamental unit of synthetic melanin: a verification by tunneling microscopy of X-ray scattering results, *BBA, Biochim. Biophys. Acta, Gen. Subj.*, 1994, **1199**(3), 271–278.
- 11 G. W. Zajac, J. M. Gallas and A. E. Alvarado-Swaisgood, Tunneling microscopy verification of an X-ray scattering-derived molecular model of tyrosine-based melanin, *J. Vac. Sci. Technol., B: Microelectron. Nanometer Struct.-Process., Meas., Phenom.*, 1994, **12**(3), 1512–1516.
- 12 M. Arzillo, G. Mangiapia, A. Pezzella, R. K. Heenan, A. Radulescu, L. Paduano, *et al.*, Eumelanin buildup on the nanoscale: aggregate growth/assembly and visible absorption development in biomimetic 5,6-dihydroxyindole polymerization, *Biomacromolecules*, 2012, **13**(8), 2379–2390.
- 13 C. M. Clancy, J. B. Nofsinger, R. K. Hanks and J. D. Simon, A Hierarchical Self-Assembly of Eumelanin, *J. Phys. Chem. B*, 2000, **104**, 7871–7873.
- 14 C. M. Clancy and J. D. Simon, Ultrastructural Organization of Eumelanin from Sepia Officinalis Measured by Atomic Force Microscopy, *Biochemistry*, 2001, **40**, 13353–13360.
- 15 L. Yan and J. D. Simon, The Effect of Preparation Procedures on the Morphology of Melanin from the Ink Sac of Sepia officinalis, *Pigm. Cell Res.*, 2003, **16**, 72–80.
- 16 L. Yan and J. D. Simon, Isolation and Biophysical Studies of Natural Eumelanins: Applications of Imaging Technologies and Ultrafast Spectroscopy, *Pigm. Cell Melanoma Res.*, 2003, **16**, 606–618.
- 17 Y. Liu, V. R. Kempf, J. B. Nofsinger, E. E. Weinert, M. Rudnicki, K. Wakamatsu, *et al.*, Comparison of the structural and physical properties of human hair eumelanin following enzymatic or acid/base extraction, *Pigm. Cell Res.*, 2003, **16**(4), 355–365.
- 18 A. Mbonyiryivuze, Y. Z. Nuru, B. D. Ngom, B. W. Mwakikunga, M. S. Dhlamini, E. Park, *et al.*, Morphological and Chemical Composition Characterization of Commercial Sepia Melanin, *Am. J. Nanomater.*, 2015, **3**(1), 22–27.
- 19 M. Magarelli, P. Passamonti and C. Renieri, Purification, characterization and analysis of sepiia melanin from commercial sepiia ink (Sepia Officinalis), *Revista CES Medicina Veterinaria y Zootecnia*, 2010, **5**(2), 18–28.
- 20 A. Camus, M. Reali, M. Rozel, M. Zhuldybina, F. Soavi and C. Santato, High conductivity Sepia melanin ink films for environmentally benign printed electronics, *Proc. Natl. Acad. Sci. U. S. A.*, 2022, **119**(32), e2200058119.



21 D. Neusser, C. Malacrida, M. Kern, Y. M. Gross, J. van Slageren and S. Ludwigs, High conductivities of disordered P3HT films by an electrochemical doping strategy, *Chem. Mater.*, 2020, **32**(14), 6003–6013.

22 Z. Wang, Characterization and Optimization of the Electrical Conductivity of a Semi-crystalline Conjugated Polymer PBTTT upon Doping, *J. Phys.: Conf. Ser.*, 2020, **1635**(1), 012037.

23 M. Wong-Stringer, J. E. Bishop, J. A. Smith, D. K. Mohamad, A. J. Parnell, V. Kumar, *et al.*, Efficient perovskite photovoltaic devices using chemically doped PCDTBT as a hole-transport material, *J. Mater. Chem. A*, 2017, **5**(30), 15714–15723.

24 J. B. Nofsinger, S. E. Forest, L. M. Eibest, K. A. Gold and J. D. Simon, Probing the building blocks of eumelanins using scanning electron microscopy, *Pigm. Cell Res.*, 2000, **13**(3), 179–184.

25 A. A. Watt, J. P. Bothma and P. Meredith, The supramolecular structure of melanin, *Soft Matter*, 2009, **5**(19), 3754–3760.

26 A. Büngeler, B. Hämisch and O. I. Strube, The supramolecular buildup of eumelanin: Structures, mechanisms, controllability, *Int. J. Mol. Sci.*, 2017, **18**(9), 1901.

27 Y. Li, J. Liu, Y. Wang, H. W. Chan, L. Wang and W. Chan, Mass spectrometric and spectrophotometric analyses reveal an alternative structure and a new formation mechanism for melanin, *Anal. Chem.*, 2015, **87**(15), 7958–7963.

